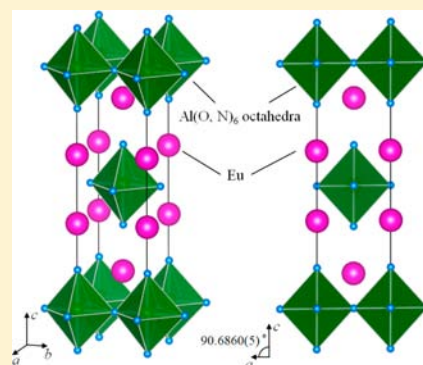


Crystal Structures and Properties of Europium Aluminum Oxynitride $\text{Eu}_2\text{AlO}_{3.75}\text{N}_{0.1}$ and Europium Aluminum Oxide EuAl_2O_4 Keitaro Tezuka,^{*,†} Yoshimi Tokuhara,[†] Makoto Wakeshima,[‡] Yue Jin Shan,[†] Hideo Imoto,[†] and Yukio Hinatsu[‡][†]Department of Material and Environmental Chemistry, Graduate School of Engineering, Utsunomiya University, 7-1-2 Yoto, Utsunomiya 321-8585, Japan[‡]Division of Chemistry, Graduate School of Science, Hokkaido University, Sapporo 060-0810, Japan

Supporting Information

ABSTRACT: The reactions among Eu_2O_3 , AlN , and Al_2O_3 with the ratios $\text{Eu}:\text{Al} = 2:1$ and $1:2$ at $1200\text{ }^\circ\text{C}$ for 10 h yielded $\text{Eu}_2\text{AlO}_{3.75}\text{N}_{0.1}$ and EuAl_2O_4 , respectively. The powder X-ray diffraction pattern of the new oxynitride could be indexed as a monoclinic structure with the space group $I2$ (No. 5) ($a = 3.7113(2)\text{ \AA}$, $b = 3.6894(2)\text{ \AA}$, $c = 12.3900(8)\text{ \AA}$, and $\beta = 90.6860(5)^\circ$). This structure was found to be a novel distorted Ruddlesden–Popper type. For EuAl_2O_4 , isostructural with monoclinic SrAl_2O_4 (space group $P2_1$, No. 4), a structural refinement was performed, indicating that the cell parameters were $a = 8.44478(11)\text{ \AA}$, $b = 8.82388(12)\text{ \AA}$, $c = 5.15643(7)\text{ \AA}$, and $\beta = 93.1854(12)^\circ$. ^{151}Eu Mössbauer spectra revealed that the divalent and trivalent Eu ions coexisted in $\text{Eu}_2\text{AlO}_{3.75}\text{N}_{0.1}$, while Eu ions were in the divalent state in EuAl_2O_4 . A photoluminescent mechanism due to $4f^7\ (^8S_{7/2}) \leftrightarrow 4f^65d^1$ of europium in EuAl_2O_4 was proposed on the basis of the calculated band structure, the band gap obtained from UV–vis diffuse reflectance spectra, and the photoluminescence spectra.



INTRODUCTION

Non-oxide materials have attracted attention due to their peculiar chemical and physical properties. For oxynitrides, oxide and nitride anions with close ionic radii and electronegativity values often substitute each other in the same site of the lattice, forming solid solutions.^{1–9} Among such materials, some cation-doped metal oxynitrides display luminescent properties. In particular, Si–Al–O–N system materials known as SiAlON have received increased interest as potential candidates for phosphors in commercial white light-emitting diodes (LEDs).^{5–9}

From the viewpoint of synthesizing oxynitrides and their industrial applications, studies on preparation methods are also attracting attention due to the difficulty in the synthesis process. Oxynitrides are usually synthesized by heating oxide/metal in the flow of NH_3 gas as the nitrogen source^{3,4,9} or by reaction between oxide and nitride under a high-pressure N_2 atmosphere.^{6–8,10} However, the former method is strongly influenced by the purity and the flow rate of NH_3 gas, and the latter requires a high-pressure system. Furthermore, these methods cannot control the ratio of the starting materials, and also the possible range of reaction temperatures is limited.

In order to resolve these problems, we have attempted to prepare new oxynitrides by reactions between oxides and nitrides in a silica tube. A similar technique has been widely applied to preparations of non-oxide materials such as sulfides.^{11–14} The encapsulation syntheses of some oxynitrides have also been reported, mainly using an evacuated nickel

tube.^{15,16} When metal oxide and nitride are heated together in an evacuated closed system, we can expect two types of reactions. One is the reaction between oxide and nitride to form oxynitride. Another is the decomposition of the starting nitride, resulting in the formation of low-valent oxides or oxynitrides. In particular, the latter reaction is peculiar to this technique, and unique compounds are expected to be prepared by selecting appropriate starting materials and preparation conditions.

In this study, we have chosen the Eu–Al compounds as the target system and succeeded in obtaining a new oxynitride, $\text{Eu}_2\text{AlO}_{3.75}\text{N}_{0.1}$, and the photoluminescent EuAl_2O_4 .

EXPERIMENTAL SECTION

Europium sesquioxide (Eu_2O_3 , Nippon Yttrium, 99.9%), aluminum mononitride (AlN), and alumina (Al_2O_3 , Kanto Chemical, 99%) were used as starting materials. The AlN compound was prepared by heating powders of Al (Kojundo Chemical Laboratory, 99.9%) at $1100\text{ }^\circ\text{C}$ for 10 h in the flow of NH_3 gas. The mixture of starting materials was ground, pressed into a pellet, and sealed in an evacuated silica tube. The tube was heated at $1200\text{ }^\circ\text{C}$ for 10 h.

Powder X-ray diffraction (XRD) measurements were carried out with $\text{Cu K}\alpha$ radiation on a RINT2200 diffractometer (Rigaku) equipped with a graphite monochromator. The Eu oxidation states were investigated through the ^{151}Eu Mössbauer spectrum measurements with a VT-6000 (Labo. Equip. Co., Japan). Quantitative analysis

Received: May 30, 2013

Published: November 5, 2013



of nitrogen and oxygen in a prepared sample was performed with the oxygen/nitrogen combustion analyzer EMGA-920 (Horiba). Quantitative analysis of the cation composition was performed with a wavelength-dispersive X-ray fluorescence (XRF) spectrometer, ZSX PrimusII (Rigaku). Thermogravimetric (TG) analysis for the product EuAl_2O_4 was performed with the Bruker TG-DTA 2000S system. The sample and reference (Al_2O_3) were placed in Pt cells heated in air to 1000 °C at a rate of 5 °C/min and maintained for 6 h. The optical second-harmonic generation (SHG) responses were tested for the compounds using a Continuum Minilite YAG:Nd laser (λ 1064 nm). UV–vis diffuse reflectance spectra were measured with a V-570 instrument (JASCO). Photoluminescence spectra were measured on the same spectrometer in the range from excitation wavelength plus 20 to 700 nm. The detection of photoluminescence was tried with excitation light at wavelengths of 220, 250, 300, 350, 400, 450, and 500 nm.

Rietveld analysis was performed using the program RIETAN-FP.¹⁷ The crystal structures were visualized with the program VESTA.¹⁸ The calculations of the electronic structures, densities of states (DOS), and quadrupole coupling constants for EuAl_2O_4 were carried out using the WIEN2k program package.¹⁹ This program employs the full potential linearized augmented plane wave + local orbitals (FP-LAPW + lo) method based on density functional theory (DFT). We used the generalized gradient approximation (GGA) + Hubbard U parameter for the Eu 4f electrons. In the calculation, the convergence parameter was set to be $R_{\text{MT}}k_{\text{max}} = 7.0$, and the muffin-tin (MT) spheres are $R_{\text{MT}}(\text{Eu}) = 2.30$ bohr, $R_{\text{MT}}(\text{Al}) = 1.42$ bohr, and $R_{\text{MT}}(\text{O}) = 1.73$ bohr. We used $8 \times 8 \times 14$ meshes, which generated 224 k points in the first Brillouin zone.

RESULTS AND DISCUSSION

In this study, the ratios of Eu:Al were investigated for 2:1 and 1:2. In the case of Eu:Al = 2:1, a new oxynitride named Eu2–Al1–O–N was obtained, and its composition and crystal structure were investigated. For Eu:Al = 1:2, EuAl_2O_4 , known as a luminescent material, was prepared, and its characterizations were performed. The crystal structure of EuAl_2O_4 was determined for the first time.

Preparation of Eu2–Al1–O–N. The reactions with the mixing ratio $\text{Eu}_2\text{O}_3:\text{AlN} = 1:1$ (Eu:Al = 2:1) were investigated with the silica tube technique. The XRD patterns of the Eu2–Al1–O–N phase are shown in Figure 1. The pattern of the new phase is similar to that of $\text{Eu}_2\text{AlO}_3\text{N}$, and other impurity phases are also observed, as shown in Figure 1a. The products were obtained as a pellet, and part of the surface was covered by

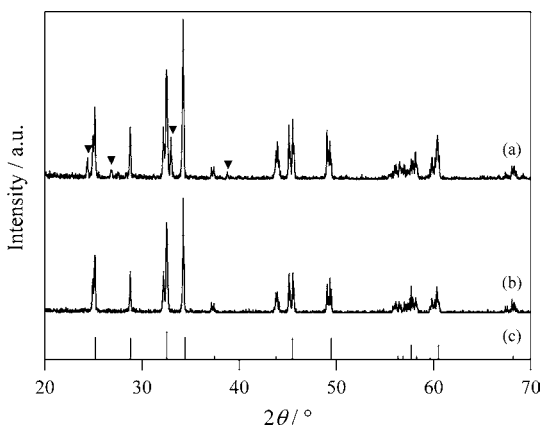


Figure 1. XRD patterns of (a) Eu2–Al1–O–N with the orange impurity phase and (b) pure Eu2–Al1–O–N and reported patterns of (c) $\text{Eu}_2\text{AlO}_3\text{N}$ (JCPDS Card No. 47-0099). Solid inverted triangles show the main peaks of the impurity phase.

orange impurities, which could not be identified. The impurities were removed from the pellet by using sandpaper, and the pure phase Eu2–Al1–O–N was obtained, which was black, having no photoluminescent properties. Silicon in the quartz tube often reacts with the sample to form silicon compounds. However, the silicon concentration in the product was below the detection limit of the XRF measurement. The compositions of oxygen and nitrogen were determined to be 15.3 and 0.4 mass %, respectively, by combustion analysis. These results with the condition of Eu:Al = 2:1 gave the empirical formula $\text{Eu}_2\text{AlO}_{3.75}\text{N}_{0.1}$, in which the average oxidation state of Eu was calculated to be 2.4.

The Eu:Al ratio was maintained at 2:1 in the product, because the Eu:Al ratio of the product agreed well with that of the mixture in the molar ratio $\text{Eu}_2\text{O}_3:\text{AlN} = 1:1$ through the XRF measurements. An amorphous phase of Al compounds is often formed as impurities of a crystalline compound. If such an amorphous Al compound exists, the main product should have Al deficiencies. However, an Al deficiency is not observed from the Rietveld analysis. Then, with the aim of investigating the phase stability and composition of the product, we attempted to prepare Eu_2AlO_4 using stoichiometric starting materials Eu_2O_3 , Al_2O_3 , and Al without AlN. As a result, the Ruddlesden–Popper (layered perovskite) phase was not observed at all. Furthermore, preparations of compositions $\text{Eu}_2\text{AlO}_{3.75}$ and $\text{Eu}_2\text{AlO}_{3.90}$ having the ratio $\text{Eu}^{\text{II}}:\text{Eu}^{\text{III}} = 3:2$ were also tried in the same way. In both XRD patterns, impurities with considerable peak intensities were detected in addition to a Ruddlesden–Popper phase. From these results, we conclude that the composition of Eu2–Al1–O–N is determined to be $\text{Eu}_2\text{AlO}_{3.75}\text{N}_{0.1}$. The amount of the anion deficiency of $\text{Eu}_2\text{AlO}_{3.75}\text{N}_{0.1}$ is as large as that for the Ruddlesden–Popper phase. Such a large amount of the anion deficiency was found to exist in $\text{Nd}_{1.8}\text{Sr}_{0.72}\text{NiO}_{3.72}$.²⁰ In the case of $\text{Eu}_2\text{AlO}_{3.75}\text{N}_{0.1}$, the existence of nitrogen and a large anion deficiency would stabilize a Ruddlesden–Popper phase.

Although the XRD profile of the pure phase was similar to that of tetragonal $\text{Eu}_2\text{AlO}_3\text{N}$,²¹ most of the diffraction peaks split and the pattern could be indexed with the monoclinic system (see Figure 1b,c). Then, instead of Eu, Sm and Gd, which are neighbors of Eu in the periodic table, were used as the oxide for the reactions with AlN in order to elucidate the tendency of the phase formation. The XRD patterns of the products did not show any phase similar to the pattern of Eu2–Al1–O–N (Figure 2). Therefore, the new phase is unique to Eu, and this suggests that the formation of the new phase depends on the stability of Eu(II). Since the starting compound is the trivalent oxide Eu_2O_3 , part of the Eu is reduced during the reaction.

¹⁵¹Eu Mössbauer Spectrum of Eu2–Al1–O–N. Figure 3 shows the ¹⁵¹Eu Mössbauer spectrum of the Eu2–Al1–O–N phase. Two large absorption peaks are observed, indicating that Eu ions with two oxidation states coexist. The Eu ions occupy a 4c site of the space group $I2(C2)$, as discussed later. Because the site symmetry is 1, a nonzero quadrupole interaction is expected.²² The quadrupole interaction is given by

$$H_Q = (e^2qQ)/(4I(2I - 1))[3I_z^2 - I(I + 1) + \eta(I_x^2 - I_y^2)] \quad (1)$$

where I is the nuclear spin, Q is the quadrupole moment, $eq = V_{zz}$, and $\eta = (V_{xx} - V_{yy})/V_{zz}$ (V_{ii} is the electric field gradient tensor).²³ Since the Eu site has no symmetry, 12 possible

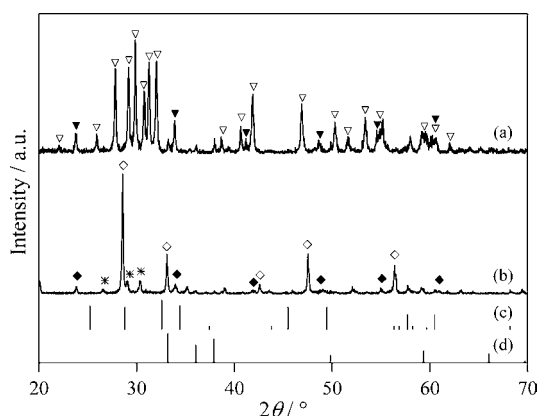


Figure 2. XRD patterns of the products obtained by the ratios (a) $\text{Sm}_2\text{O}_3:\text{AlN} = 1:1$ and (b) $\text{Gd}_2\text{O}_3:\text{AlN} = 1:1$ and reported patterns of (c) $\text{Eu}_2\text{AlO}_3\text{N}$ (JCPDS Card No. 47-0099) and (d) AlN (JCPDS Card No. 25-1133). Legend: (∇) Sm_2O_3 (JCPDS Card No. 42-1464); (\blacktriangledown) SmAlO_3 (JCPDS Card No. 29-0082); (\diamond) Gd_2O_3 (JCPDS Card No. 12-0797); (\blacklozenge) GdAlO_3 (JCPDS Card No. 46-0395); ($*$) $\text{Gd}_4\text{Al}_2\text{O}_9$ (JCPDS Card No. 46-0396).

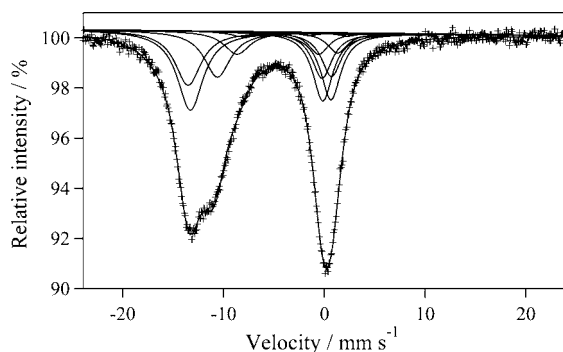
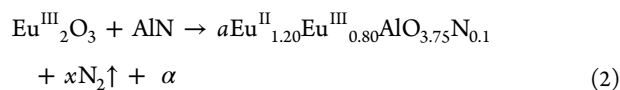


Figure 3. ^{151}Eu Mössbauer spectrum of $\text{Eu}_2\text{-Al}_1\text{-O-N}$ at 20 K.

transitions exist due to the quadrupole interaction. Thus, the spectrum was fitted by using 12 Lorentzian functions for each of the two absorption peaks. Table 1 gives the ^{151}Eu Mössbauer parameters. The isomer shifts, $-11.981(13)$ and $0.282(9)$ mm/s relative to EuF_3 , are assigned to Eu^{II} and Eu^{III} , respectively.²⁴ Since the spectrum was measured at a low temperature (20 K), the recoil-free fractions of Eu^{II} and Eu^{III} are almost equal and the ratio $\text{Eu}^{\text{II}}:\text{Eu}^{\text{III}}$ was determined to be 3.0:2.0 from the areas of the two peaks. The average oxidation number of Eu calculated from the ratio is 2.4, which is exactly the same as that estimated from the compositional analyses.

The synthesis reaction is estimated to be



where α is the composition of impurities removed from the pellet and the values of a and x are unknown because of the undetermined quantity of impurities.

Table 1. ^{151}Eu Mössbauer Parameters for $\text{Eu}_2\text{-Al}_1\text{-O-N}$ at 20 K

species	δ (mm/s)	$eV_{zz}Q_q$ (mm/s)	η	I_0 (%)	Γ (mm/s)
Eu^{II}	$-11.981(13)$	$-16.9(2)$	$0.47(2)$	$-12.70(11)$	$3.14(4)$
Eu^{III}	$0.282(9)$	$-5.6(3)$	$0.83(9)$	$-11.1(2)$	$2.41(6)$

Crystal Structure of $\text{Eu}_2\text{-Al}_1\text{-O-N}$. The crystal system was determined to be monoclinic by indexing the XRD peaks. However, all of the known compounds $\text{R}_2\text{AlO}_3\text{N}$ ($\text{R} = \text{La-Nd, Sm, Eu}$), with compositions similar to that of $\text{Eu}^{\text{II}}_{1.20}\text{Eu}^{\text{III}}_{0.80}\text{AlO}_{3.75}\text{N}_{0.1}$, have tetragonal structures with space group $I4/mmm$ or $I4mm$.^{15,21,25} These compounds crystallize in the Ruddlesden–Popper-type structure expressed by the chemical formula $\text{A}_{n+1}\text{B}_n\text{X}_{3n+1}$ ($\text{A, B} = \text{cation, X} = \text{anion}$) with $n = 1$. As the XRD peaks with reflection conditions $h + k + l = 2n$ for hkl in the unique axis b are observed, it has a body-centered lattice. Furthermore, the multiplicity of the crystallographic Al site must be equal to or less than 2 because a unit cell contains only two Al atoms. From these conditions, possible space groups are narrowed down to $I2$ (cell choice 3 of $C2$, No. 5), Im (cell choice 3 of Cm , No. 8), and $I2/m$ (cell choice 3 of $C2/m$, No. 12). These space groups can be classified into subgroup groups of $I4/mmm$. The YAG laser radiation to the powder samples showed SHG signals, indicating exclusion of centrosymmetric $I2/m$, although the intensity of the signal was weaker than that for the quartz. Space groups $I2$ and Im were investigated using the Rietveld method.

First, we attempted the space group $I2$. Initial crystal parameters of the structural refinement were referenced to those of $\text{Nd}_2\text{AlO}_3\text{N}$ ($I4mm$).²⁵ The $4c$ site (0, 0, 0.3649) is used as the initial position of Eu, assuming that Eu^{II} and Eu^{III} are located randomly. The Al site was set as the $2a$ site, (0, 0, 0). Because it is too difficult to verify the site occupancies of O and N from XRD data, O and N are assumed to occupy disordered anion sites. The anion sites were (0, 0.5, 0) of the $2a$ site, (0, 0.5, 1/2) of the $2b$ site, and (0.5, 0.5, 0.6700) of the $4c$ site. Anion vacancy is also disordered; that is, the occupancy of all these sites was uniformly 0.9625. The refined results are shown in Table 2 and Figure 4. The R_{wp} and S values converged to 8.36% and 1.30, respectively. For $\text{Nd}_2\text{AlO}_3\text{N}$, Al–O/N bonds (2.086 Å for Al–O and 2.130 Å for Al–N) perpendicular to $\text{Al}(\text{O/N})_2$ layers are obviously longer than those (1.855 Å for Al–O) parallel to the layers. The tendency of these distances is also observed in the refined structure, as shown in Table 3. In addition, three kinds of Al–O/N bonds parallel to the layers exist, and one of them (1.70(5) Å) is much shorter than the other distances (1.857(3) and 1.99(5) Å). Thus, a large distortion of $\text{Al}(\text{O/N})_6$ octahedra was observed in the monoclinic system.

Then, the space group Im was studied. The initial crystal parameters are also referenced to those for $\text{Nd}_2\text{AlO}_3\text{N}$. As all of the atoms occupy the $2a$ sites, equivalent Eu sites and O/N sites increase in number to 2 and 4, respectively. The other refinement conditions were the same as that for $I2$. The R_{wp} and S values converged to 8.33% and 1.29, respectively. A large distortion of $\text{Al}(\text{O/N})_6$ octahedra with a very short Al–O/N distance (1.700 Å) was also observed.

A significant difference between the results of $I2$ and Im was not observed. Thus, we reconsidered the result of the ^{151}Eu Mössbauer spectrum, because this is strongly affected by the coordination environment of europium. In the case of $I2$, the spectra can be analyzed using 12 Lorentzian functions for each

Table 2. Crystallographic Data for $\text{Eu}^{\text{II}}_{1.20}\text{Eu}^{\text{III}}_{0.80}\text{AlO}_{3.75}\text{N}_{0.1}$ at Room Temperature

	space group	<i>I</i> 2 (No. 5, setting 3)				
	<i>a</i> /Å	3.7113(2)				
	<i>b</i> /Å	3.6894(2)				
	<i>c</i> /Å	12.3900(8)				
	β /deg	90.6860(5)				
	$R_{\text{wp}}/\%$	8.36				
	<i>S</i>	1.30				
atom	site	<i>g</i>	<i>x</i>	<i>y</i>	<i>z</i>	<i>B</i> /Å ²
Eu	4 <i>c</i>	1.0	0.4968(2)	0.504(13)	0.85755(4)	0.607(10)
Al	2 <i>a</i>	1.0	0	0.0	0	0.88(6)
O/N1	2 <i>a</i>	0.9625	0	0.539(14)	0	0.3(2)
O/N2	2 <i>b</i>	0.9625	0	0.52(2)	1/2	1.7(2)
O/N3	4 <i>c</i>	0.9625	0.498(2)	0.51(2)	0.6660(4)	0.83(11)

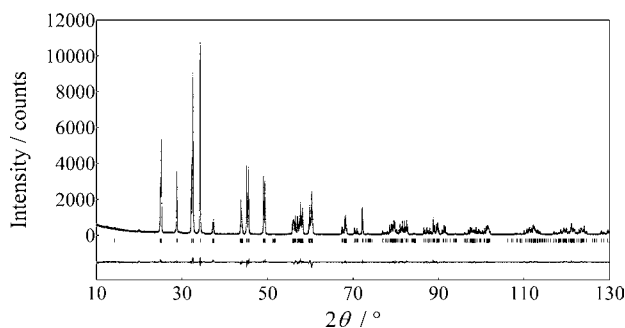


Figure 4. Powder X-ray diffraction pattern fitting for $\text{Eu}^{\text{II}}_{1.20}\text{Eu}^{\text{III}}_{0.80}\text{AlO}_{3.75}\text{N}_{0.1}$. The calculated and observed patterns are shown by the top solid line and the cross markers, respectively. The vertical marks in the middle show positions calculated for Bragg reflections. The lower trace is a plot of the difference between calculated and observed intensities.

Table 3. Selected Bond Distances of $\text{Eu}^{\text{II}}_{1.20}\text{Eu}^{\text{III}}_{0.80}\text{AlO}_{3.75}\text{N}_{0.1}$

species	distance (Å)	species	distance (Å)
Eu–O/N1	$2.5575(12) \times 1$	Eu–O/N1	$2.5710(12) \times 1$
Eu–O/N2	$2.52(5) \times 1$	Eu–O/N2	$2.59(5) \times 1$
Eu–O/N3	$2.374(5) \times 1$	Eu–O/N3	$2.61(5) \times 1$
Eu–O/N3	$2.63(5) \times 1$	Eu–O/N3	$2.64(5) \times 1$
Eu–O/N3	$2.66(5) \times 1$		
Al–O/N1	$1.70(5) \times 1$	Al–O/N1	$1.99(5) \times 1$
Al–O/N2	$1.857(3) \times 2$	Al–O/N3	$2.057(5) \times 2$

of the two absorption peaks corresponding to Eu^{II} and Eu^{III} , as shown in Table 1, due to having only one europium site. On the other hand, *Im* has two crystallographic sites for europium. In this case, Eu^{II} must occupy two sites, since the ratio $\text{Eu}^{\text{II}}:\text{Eu}^{\text{III}}$ is greater than 1. Because this analysis could not distinguish accurately the two sites, space group *I*2 having one europium crystallographic site was adopted. The refined crystal structure of $\text{Eu}^{\text{II}}_{1.20}\text{Eu}^{\text{III}}_{0.80}\text{AlO}_{3.75}\text{N}_{0.1}$ with space group *I*2 is shown in Figure 5. The basic crystal structure is confirmed to be similar to that for $\text{Eu}_2\text{AlO}_3\text{N}$.

However, this refined crystal structure differs from the previously reported Ruddlesden–Popper structures with the chemical formula A_2BX_4 . Generally, tilts with rotations of corner-sharing BX_6 octahedra yield distortions from the ideal tetragonal A_2BX_4 structure (*I*4/*mmm*).^{26,27} Recently, Harris reexamined the rigid octahedral tiltings and classified them into 10 structures using a Landau expansion of the free energy.²⁸

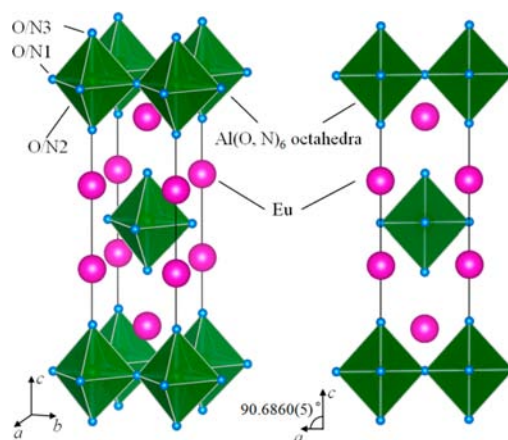
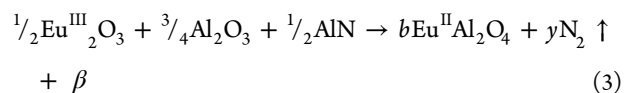


Figure 5. Crystal structure of $\text{Eu}^{\text{II}}_{1.20}\text{Eu}^{\text{III}}_{0.80}\text{AlO}_{3.75}\text{N}_{0.1}$.

For these A_2BX_4 structures, the conventional unit cell volumes ($Z \geq 4$) with octahedral tiltings are 2 times more than that of the ideal structure ($Z = 2$). On the other hand, while the crystal structure of $\text{Eu}^{\text{II}}_{1.20}\text{Eu}^{\text{III}}_{0.80}\text{AlO}_{3.75}\text{N}_{0.1}$ is distorted due to monoclinic symmetry, the number of the chemical formula per the conventional unit cell is $Z = 2$. In this structure, the $\text{Al}(\text{O}/\text{N})_6$ octahedron has a tilt with no rotation. The unique tilt of the $\text{Al}(\text{O}/\text{N})_6$ octahedron may be attributable to deficiencies and disorders between O and N anions and/or more covalent Al–O/N bonds in comparison with ionic Al–O bonds.

Preparation of EuAl_2O_4 . Although EuAl_2O_4 is known as a promising photoluminescent material with green emission,²⁹ the crystal structure has not been reported due to the difficulty in preparing a sample with good crystallinity. A pure phase of EuAl_2O_4 was obtained when the molar ratio of the starting compounds was $\text{Eu}_2\text{O}_3:\text{Al}_2\text{O}_3:\text{AlN} = 2:3:2$. From this result, the reaction is presumed to be



where β is the composition of impurities removed from the pellet, and the values of *b* and *y* are unknown because of the undetermined quantity of the impurities. In order to confirm the nitrogen amount in the product, TG analysis was performed at 1000 °C. If the chemical composition of the entire product is EuAl_2O_4 , the theoretical weight gain should be 2.96% of the product due to the chemical reaction $4\text{Eu}^{\text{II}}\text{Al}_2\text{O}_4 + \text{O}_2 \rightarrow 4\text{Eu}^{\text{III}}\text{AlO}_3 + 2\text{Al}_2\text{O}_3$. The actual weight gain is 2.96%,

which is the same as the theoretical value. Therefore, the composition of the product is determined to be EuAl_2O_4 . We also attempted to prepare EuAl_2O_4 from Eu_2O_3 , Al_2O_3 , and Al in order to clarify the effect of AlN. In the reaction, EuAlO_3 was formed as the main product with a small amount of EuAl_2O_4 . Thus, we confirmed that the use of AlN is necessary for the preparation of EuAl_2O_4 . The calculated Gibbs free energy change of the reduction reaction of Eu_2O_3 to EuO by AlN or Al indicates that AlN is not better than Al as a reducing agent.³⁰ Thus, AlN is expected not to be suitable as the starting material for the preparation of EuAl_2O_4 from the point of view of thermodynamic equilibrium. Therefore, AlN probably has a great advantage for the reaction in terms of the chemical kinetics. The reaction rates are expected to be mainly related to the particle surface conditions of AlN and Al owing to decomposition of AlN and/or passivity of Al.

Crystal Structure of EuAl_2O_4 . The XRD profile of the product shown in Figure 6 is very similar to that of SrAl_2O_4 ,³¹

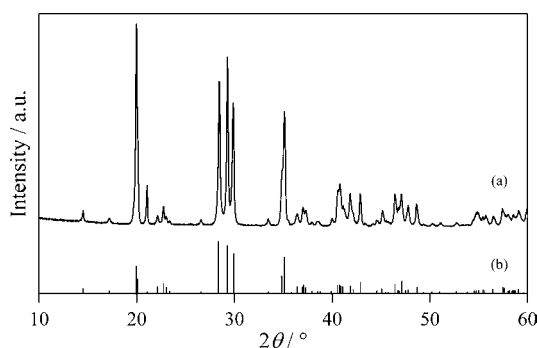


Figure 6. XRD pattern of (a) EuAl_2O_4 and reported pattern of (b) SrAl_2O_4 (JCPDS Card No. 34-0379).

suggesting that they are isostructural. The SrAl_2O_4 phase has a monoclinic structure with the space group $P2_1$ (No. 4). EuAl_2O_4 gave SHG signals, supporting the notion that it has the non-centrosymmetric space group $P2_1$. The intensity of the SHG signal for the EuAl_2O_4 was stronger than that for the quartz. Then, with the atomic parameters of SrAl_2O_4 as initial values, the structure of EuAl_2O_4 could be refined (Table 4 and Figure 7). The R_{wp} and S values converged to 6.45% and 1.31, respectively. The refined crystal structure is shown in Figure 8, and selected bond distances are given in Table 5. The cell parameters of EuAl_2O_4 ($a = 8.44478(11)$ Å, $b = 8.82388(12)$ Å, $c = 5.15643(7)$ Å, and $\beta = 93.1854(12)^\circ$) are very close to those of SrAl_2O_4 ($a = 8.447$ Å, $b = 8.816$ Å, $c = 5.163$ Å, and $\beta = 93.42^\circ$),³¹ due to the almost identical ionic radii of Eu^{2+} and Sr^{2+} . The Al–O and Eu–O lengths are also similar to those for SrAl_2O_4 (1.730–1.772 Å for Al–O, 2.508–3.114 Å for Sr–O). The bond valence sum (BVS) method was applied to estimate the valence of cations using $r_0(\text{Eu}^{2+}-\text{O}^{2-}) = 2.147$ Å and $r_0(\text{Al}^{3+}-\text{O}^{2-}) = 1.644$ Å. The calculated bond valences for Eu1 and Eu2 were +1.78 and +1.84, respectively. These values are similar to those expected for divalent europium and are consistent with the result obtained from Mössbauer spectra, as mentioned later. The calculated bond valences for Al1, Al2, Al3, and Al4 were +3.26, +3.09, +2.79, and +2.99, respectively, indicating that aluminum is in a trivalent state.

^{151}Eu Mössbauer Spectrum of EuAl_2O_4 . As described above, Eu atoms in EuAl_2O_4 occupy two crystallographic sites with no symmetry elements, and the ^{151}Eu Mössbauer spectrum consists of 2 sets of 12 overlapping peaks due to quadrupole

Table 4. Crystallographic Data for EuAl_2O_4 at Room Temperature^a

space group	$P2_1$ (No. 4, setting 1)				
$a/\text{Å}$	8.44478(11)				
$b/\text{Å}$	8.82388(12)				
$c/\text{Å}$	5.15643(7)				
β/deg	93.1854(12)				
$R_{\text{wp}}/\%$	6.45				
S	1.31				
atom	site	x	y	z	$B/\text{Å}^2$
Eu1	2a	0.4926(2)	0.0	0.2517(3)	0.66(5)
Eu2	2a	0.0267(2)	0.9928(3)	0.2005(3)	0.57(5)
Al1	2a	0.1935(13)	0.8178(11)	0.709(2)	0.68(8)
Al2	2a	0.8014(14)	0.8317(11)	0.738(2)	0.68(8)
Al3	2a	0.7034(14)	0.6576(12)	0.235(2)	0.68(8)
Al4	2a	0.6837(13)	0.1656(13)	0.798(2)	0.68(8)
O1	2a	0.270(2)	0.185(2)	0.428(4)	0.47(12)
O2	2a	0.738(2)	0.334(2)	0.599(4)	0.47(12)
O3	2a	0.3239(12)	0.502(3)	0.344(2)	0.47(12)
O4	2a	0.2633(13)	0.975(2)	0.879(2)	0.47(12)
O5	2a	0.170(2)	0.294(2)	0.936(3)	0.47(12)
O6	2a	0.217(2)	0.665(2)	0.891(3)	0.47(12)
O7	2a	0.489(2)	0.221(2)	0.874(2)	0.47(12)
O8	2a	0.992(2)	0.877(2)	0.635(3)	0.47(12)

^aFitting of the isotropic atomic displacement parameters, B , of Al and O was carried out as one kind, respectively.

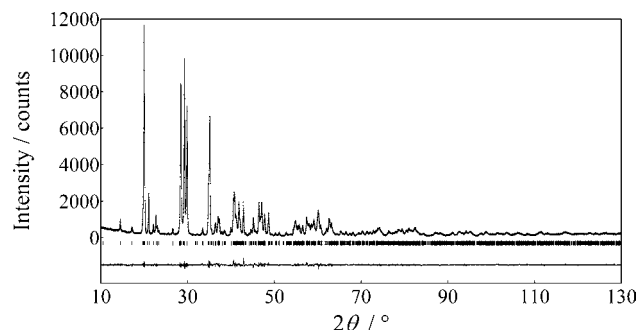


Figure 7. Powder X-ray diffraction pattern fitting for EuAl_2O_4 . The calculated and observed patterns are shown by the top solid line and the cross markers, respectively. The vertical marks in the middle show positions calculated for Bragg reflections. The lower trace is a plot of the difference between calculated and observed intensities.

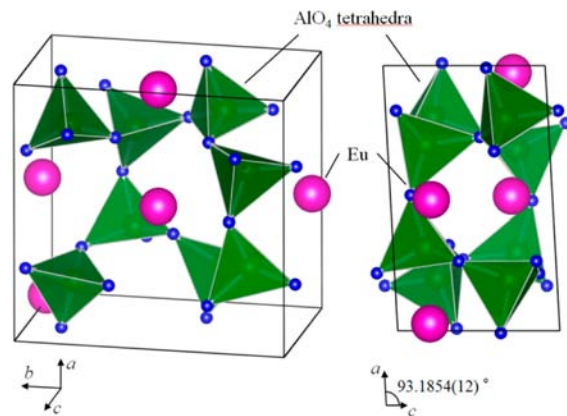


Figure 8. Crystal structure of EuAl_2O_4 .

Table 5. Selected Bond Distances of EuAl_2O_4

bond	distance (Å)	bond	distance (Å)
Eu1–O1	2.69(2)	Eu2–O1	2.87(2)
Eu1–O2	2.59(2)	Eu2–O2	2.60(2)
Eu1–O3	2.527(11)	Eu2–O4	2.670(11)
Eu1–O4	2.661(11)	Eu2–O5	2.49(2)
Eu1–O6	2.977(13)	Eu2–O6	2.58(2)
Eu1–O7	2.56(2)	Eu2–O8	2.499(14)
Eu1–O7	2.754(14)	Eu2–O8	3.088(14)
Al1–O2	1.73(2)	Al3–O1	1.75(2)
Al1–O4	1.73(2)	Al3–O4	1.74(2)
Al1–O6	1.65(2)	Al3–O5	1.86(2)
Al1–O8	1.80(2)	Al3–O7	1.78(2)
Al2–O1	1.65(2)	Al4–O2	1.88(2)
Al2–O3	1.87(2)	Al4–O3	1.62(2)
Al2–O5	1.72(2)	Al4–O6	1.77(2)
Al2–O8	1.76(2)	Al4–O7	1.79(2)

interactions. Since it was too difficult to estimate the ^{151}Eu Mössbauer parameters adequately, we used the quadrupole coupling constants and asymmetry parameters obtained from the DFT calculations as the initial parameters in Table 6 (see

Table 6. Quadrupole Coupling Constants and Asymmetry Parameters for the Eu Ions of EuAl_2O_4 Calculated Using WIEN2k^a

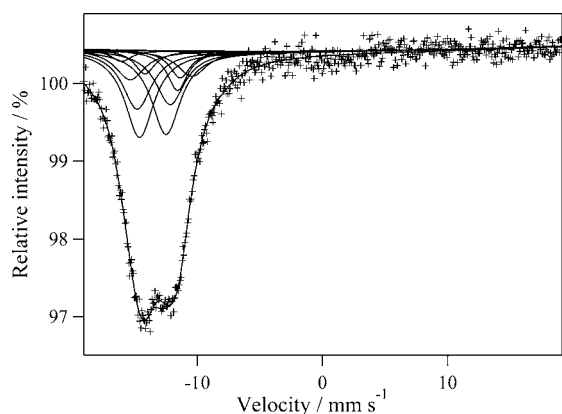
species	$eV_{zz}Q_q$ (mm/s)	η
Eu(1)	−20.1	0.65
Eu(2)	17.7	0.50

^aThe Hubbard U parameter is set at 8.2 eV.

Table 7. ^{151}Eu Mössbauer Parameters for EuAl_2O_4 at Room Temperature

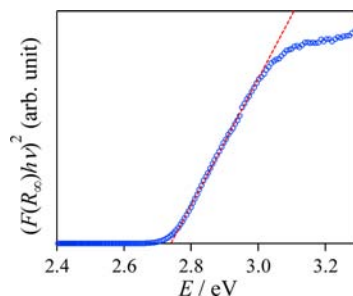
species	δ (mm/s)	$eV_{zz}Q_q$ (mm/s)	η	I_0 (%)	Γ (mm/s)
Eu(1)	−13.40(10)	−15.6(4)	0.65(16)	4.5(10)	2.84(12)
Eu(2)	−12.83(13)	16.4(8)	0.51(15)	2.1(10)	2.0(5)

the section of band structure of EuAl_2O_4). Table 7 shows the Mössbauer parameters obtained by fittings of 2 sets of 12 Lorentzian functions to the observed data in Figure 9. The

Figure 9. ^{151}Eu Mössbauer spectrum of EuAl_2O_4 at room temperature.

isomer shifts relative to EuF_3 of the Eu(1) and Eu(2) sites were determined to be $-13.40(10)$ and $-12.83(13)$ mm/s, respectively, and they confirmed that all Eu ions were in the divalent state.

Band Structure of EuAl_2O_4 . Figure 10 shows the UV–vis diffuse reflectance spectrum. The absorption coefficients were

Figure 10. Diffuse reflectance spectrum of EuAl_2O_4 . The Tauc plot is shown.

calculated from the reflectance data with the Kubelka–Munk function.³² The energy of the optical band gap was determined to be 2.74 eV from the Tauc plot (see Figure 10).³³ The fact that the photon energy ($h\nu$) is proportional to the square of $F(R_\infty)h\nu$ indicates the predominance of the direct, allowed transition, in agreement with the result of our DFT calculations (see below).

In the DFT calculations of insulators with strongly correlated electrons, the energy of the band gap is very sensitive to the Hubbard U parameter. In the case of EuAl_2O_4 , the band gap energy E_g calculated with the WIEN2k program increased with the U parameter. Thus, we adjusted the U parameter so that the calculated E_g value became equal to the observed value (2.7 eV), and it was determined to be 8.2 eV. Figure 11a shows the total density of states and partial DOS for Eu 4f electrons and total electrons of Eu, Al, and O. From the partial DOS, it is found that the top of the valence band located from -0.5 to 0 eV primarily consists of up-spin states of Eu 4f and O 2p orbitals, while the lowest unoccupied state in the conduction band is mainly composed of hybridized states between O 2p and Eu 5d orbitals. Figure 11b,c shows the energy dispersions for the up-spin and down-spin states, respectively. The dispersions reveal that the lowest state in the conduction band is located at the Γ point and that the tops of the valence band are positioned at the X point. However, the difference between the highest energies at the Z and Γ points is small (<0.01 eV) because of the flatness of the valence band, suggesting the predominance of the direct, allowed transition ($\Gamma \rightarrow \Gamma$) in the photoluminescent properties.

Photoluminescent Properties of EuAl_2O_4 . The photoluminescent properties were measured on powder samples of pure $\text{Eu}^{\text{II}}\text{Al}_2\text{O}_4$. Figure 12 shows the excitation and emission spectra. A peak is observed at 515 nm in the emission spectrum, and two peaks are shown at around 380 nm and at 430 nm in the excitation spectra. The result of emission is consistent with earlier studies.^{29,34,35} On the other hand, the feature of the excitation spectra in our study differs from those by Zorenko et al.³⁴ and Meister et al.³⁵ More than two peaks are visible in these spectra measured using non-single-phase EuAl_2O_4 including some impurities such as EuAlO_3 and Al_2O_3 . However, it is considered that the peaks at 380 and 430 nm observed in Figure 12 are both due to intrinsic optical excitations in

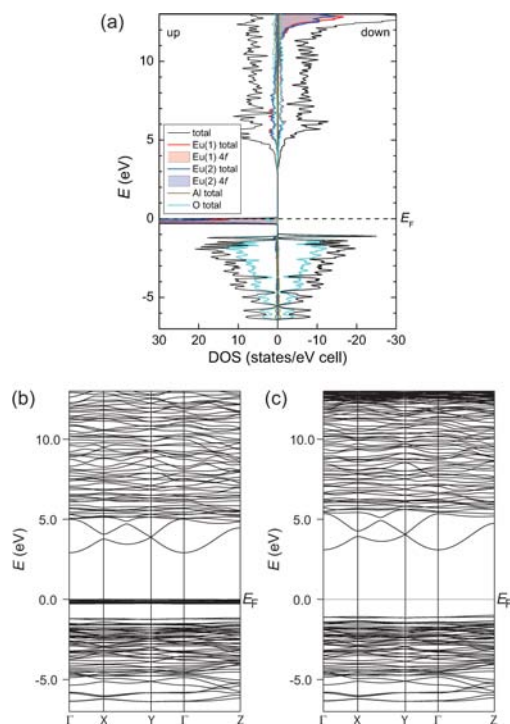


Figure 11. Total and partial density of states (DOS) (a) and energy dispersions of EuAl_2O_4 for the up-spin electrons (b) and for the down-spin electrons (c). The zero energy is placed at the highest occupied state.

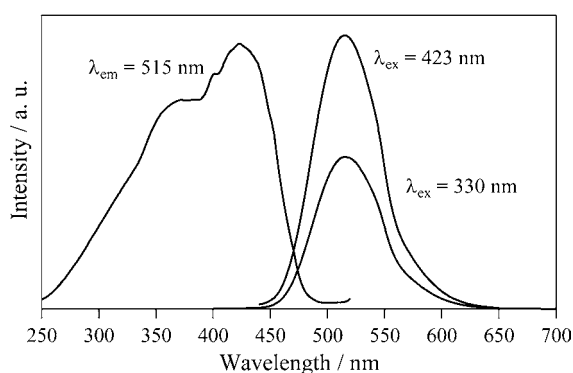


Figure 12. Excitation spectrum of luminescence at 515 nm and emission spectra under excitation at 423 and 330 nm of EuAl_2O_4 .

EuAl_2O_4 , because the normalized intensities of the peaks at 380 and 460 nm increase with Eu concentration in $\text{Eu}_x\text{Sr}_{1-x}\text{Al}_2\text{O}_4$ solid solutions.³⁵

Figure 13 illustrates a possible luminescence mechanism for EuAl_2O_4 . From the DOS and the energy dispersions in the

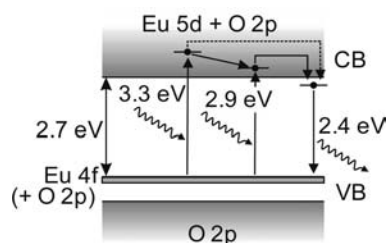


Figure 13. Luminescence mechanism for EuAl_2O_4 .

band structure of EuAl_2O_4 (see Figure 11), the excitation at 430 nm ($E \approx 2.9$ eV) and the emission at 515 nm ($E \approx 2.4$ eV) are attributable to the direct, allowed transitions ($4f^7$ ($^8S_{7/2}$) \leftrightarrow $4f^65d^1$) between Eu 4f valence bands (VBs) and conduction bands (CBs) by hybridization with O 2p and Eu 5d orbitals near the Γ point. The emission (430 nm) via the excitation at 380 nm ($E \approx 3.3$ eV) was reported to disappear due to energy transfer to the emission at 515 nm.³⁶ It is supposed that the origin of the excitation at 380 nm is also related to the transitions from the Eu 4f VB to the O 2p and Eu 5d CBs. This model accounts for the luminescence mechanism for EuAl_2O_4 .

CONCLUSIONS

We succeeded in synthesizing the new compound $\text{Eu}_2\text{AlO}_{3.75}\text{N}_{0.1}$ and the phosphor EuAl_2O_4 by reactions among Eu_2O_3 , AlN, and Al_2O_3 at 1200 °C in evacuated silica tubes. The decomposition of the aluminum nitride in the tubes induced the formations of these compounds with lower valent cations, Eu^{2+} . This novel silica tube technique should be useful in forming such low-valent oxides and oxynitrides.

For $\text{Eu}_2\text{AlO}_{3.75}\text{N}_{0.1}$, the ratio $\text{Eu}^{\text{II}}:\text{Eu}^{\text{III}}$ was determined to be 3.0:2.0 from the ^{151}Eu Mössbauer spectrum, and it has a novel Ruddlesden–Popper-type structure with monoclinic space group $I2$.

The crystal structure of EuAl_2O_4 is almost the same as that of SrAl_2O_4 with monoclinic space group $P2_1$. An emission peak of the photoluminescence was observed around 515 nm, and excitation peaks were observed around 430 nm with a shoulder around 370 nm. The excitations and the emissions are explicable in terms of the direct, allowed transitions ($4f^7$ ($^8S_{7/2}$) \leftrightarrow $4f^65d^1$) from the calculated band structures and the measured band gap.

ASSOCIATED CONTENT

Supporting Information

CIF files giving structural data of $\text{Eu}_2\text{AlO}_{3.75}\text{N}_{0.1}$ and EuAl_2O_4 . This material is available free of charge via the Internet at <http://pubs.acs.org>.

AUTHOR INFORMATION

Corresponding Author

*E-mail for K.T.: ktez@cc.utsunomiya-u.ac.jp.

Notes

The authors declare no competing financial interest.

ACKNOWLEDGMENTS

This work was partially supported by a research grant from The Murata Science Foundation and Japan Science and Technology Agency (JST), A-step feasibility study program (No. 221Z03361).

REFERENCES

- (1) Fuentes, A. *Dalton Trans.* **2010**, 39, 5942–5948.
- (2) Tessier, F.; Maillard, P.; Chevire, F.; Domen, K.; Kikkawa, S. *J. Ceram. Soc. Jpn.* **2009**, 117, 1–5.
- (3) Maeda, K.; Takata, T.; Hara, M.; Saito, N.; Inoue, Y.; Kobayashi, H.; Domen, K. *J. Am. Chem. Soc.* **2005**, 127, 8286–8287.
- (4) Kim, Y.; Woodward, P. M.; Baba-Kishi, K. Z.; Tai, C. W. *Chem. Mater.* **2004**, 16, 1267–1276.
- (5) Schnick, W. *Int. J. Inorg. Mater.* **2001**, 3, 1267–1272.
- (6) Xie, R.; Hirosaki, N.; Sakuma, K.; Yamamoto, Y.; Mitomo, M. *Appl. Phys. Lett.* **2004**, 84, 5404–5406.

- (7) Hirosaki, N.; Xie, R.; Kimoto, K.; Sekiguchi, T.; Yamamoto, Y.; Suehiro, T.; Mitomo, M. *Appl. Phys. Lett.* **2005**, *86*, 211905-1–211905-3.
- (8) Kimura, N.; Sakuma, K.; Hirafune, S.; Asano, K.; Hirosaki, N.; Xie, R. *Appl. Phys. Lett.* **2007**, *90*, 051109-1–051109-3.
- (9) Kasahara, A.; Nukumizu, N.; Hitoki, G.; Takata, T.; Kondo, J. N.; Hara, M.; Kobayashi, H.; Domen, K. *J. Phys. Chem. A* **2002**, *106*, 6750–6753.
- (10) Takahashi, J.; Yamane, H.; Hirosaki, N.; Yamamoto, Y.; Mitomo, M.; Shimada, M. *J. Eur. Ceram. Soc.* **2005**, *25*, 793–799.
- (11) Tezuka, K.; Shan, Y.; Imoto, H.; Ohoyama, K. *J. Phys. Chem. Solids* **2007**, *68*, 2133–2137.
- (12) Sunshine, S. A.; Steven, A.; Kang, D.; Ibers, J. A. *J. Am. Chem. Soc.* **1987**, *109*, 6202–6204.
- (13) Hua-Jun, Z.; Long-Hua, L.; Li-Ming, W.; Ling, C. *Inorg. Chem.* **2010**, *49*, 5811–5817.
- (14) Wada, H.; Onoda, M.; Nozaki, H. *J. Solid State Chem.* **1992**, *97*, 29–35.
- (15) Marchand, R. *C. R. Seances Acad. Sci., Ser. C: Sci. Chim.* **1976**, *282*, 329–331.
- (16) Clarke, S. J.; Hardstone, K. A.; Michie, C. W.; Rosseinsky, M. J. *Chem. Mater.* **2002**, *14*, 2664–2669.
- (17) Izumi, F.; Momma, K. *Solid State Phenom.* **2007**, *130*, 15–20.
- (18) Momma, K.; Izumi, F. *J. Appl. Crystallogr.* **2011**, *44*, 1272–1276.
- (19) Blaha, P.; Schwarz, K.; Sorantin, P.; Trickey, S. B. *Comput. Phys. Commun.* **1990**, *59*, 399–415.
- (20) Medarde, M.; Rodríguez-Carvajal, J.; Vallet-Regí, M.; González-Calbet, J. M.; Alonso, J. *Phys. Rev. B* **1994**, *49*, 8591–8599.
- (21) Huang, Z. K.; Yan, D. S.; Tien, T. Y. *J. Solid State Chem.* **1990**, *85*, 51–55.
- (22) Gütlich, P.; Link, R. *Trautwein Electric Hyperfine Interaction. In Mössbauer Spectroscopy and Transition Metal Chemistry*; Becke, M., Jørgensen, C. K., Lappert, M. F., Lippard, S. J., Margrave, J. L., Niedenzu, K., Parry, R. W., Yamatera, H., Eds.; Springer-Verlag: Berlin, 1978; *Inorganic Chemistry Concepts*; Vol. 3, pp 13–40.
- (23) Slichter, C. P. *Electric Quadrupole Effects. In Principles of Magnetic Resonance*; Harper & Row: New York, 1963; pp 160–176.
- (24) Bauminger, E. R.; Kalvius, G. M.; Nowik, I. *Isomer Shifts in the Rare Earth. In Mössbauer Isomer Shifts*; Shenoy, G. K., Wagner, F. E., Eds.; North-Holland: Amsterdam, 1978; pp 661–756.
- (25) Marchand, R.; Pastuszak, R.; Laurent, Y.; Roult, G. *Rev. Chim. Miner.* **1982**, *19*, 684–689.
- (26) Hatch, D. M.; Stokes, H. T. *Phys. Rev. B* **1987**, *35*, 8509–8516.
- (27) Hatch, D. M.; Stokes, H. T. *Phys. Rev. B* **1989**, *39*, 9282–9288.
- (28) Harris, A. B. *Phys. Rev. B* **2012**, *85*, 174107-1–22.
- (29) Schierning, G.; Batentschuk, M.; Osvet, A.; Stiegelschmitt, A.; Winnacker, A. *Phys. Status Solidi* **2005**, *2*, 109–112.
- (30) Binnewies, M.; Mike, E. *Thermochemical Data of Elements and Compounds*; 2nd ed.; Wiley-VCH: Weinheim, Germany, 2002; pp 23–699.
- (31) Schulze, A. R.; Buschbaum, H. M. *Z. Anorg. Allg. Chem.* **1981**, *475*, 205–210.
- (32) Kubelka, P.; Munk, F. Z. *Tech. Phys.* **1931**, *12*, 593–601.
- (33) Tauc, J.; Grigorovici, R.; Vancu, A. *Phys. Status Solidi* **1966**, *15*, 627–637.
- (34) Zorenko, Y.; Gorbenko, V.; Grinberg, M.; Tuross-Matysiak, R.; Kukliński, B. *Radiat. Meas.* **2007**, *42*, 652–656.
- (35) Meister, F.; Batentschuk, M.; Dröschner, S.; Osvet, A.; Stiegelschmitt, A.; Weinder, M.; Winnacker, A. *Radiat. Meas.* **2007**, *42*, 771–774.
- (36) Poort, S. H. M.; Blokpoel, W. P.; Blasse, G. *Chem. Mater.* **1995**, *7*, 1547–1551.